Proceedings of the 2007 IEEE
International Conference on Robotics and Biomimetics
December 15 -18, 2007, Sanya, China

Optimal Motion Planning of A One-Legged Hopping Robot *

Guang-Ping He
State Key Laboratory for Turbulence and Complex Systems, Department of Mechanics and Aerospace Engineering Peking University Beijing, China.
hegp55@126.com

Zhi-Yong Geng
State Key Laboratory for Turbulence and Complex Systems, Department of Mechanics and Aerospace Engineering Peking University Beijing, China.
zygeng@pku.edu.cn

***Abstract* - The optimal motion planning and stable jumping control for a new one-legged hopping robot are investigated. The new robot has one passive telescopic leg and two actuated arms, therefore an underactuated mechanical system of which the motion can only be controlled by the internal dynamic coupling. The features of the dynamic coupling between the passive leg and the actuated arms are analyzed through measuring two proposed indices. An optimal motion planning algorithm is introduced for maximizing energy efficiency of the motion of the robot. The feasibility of the optimal motion-planning algorithm is verified by some numerical simulations in which varying height and varying moving speed are considered.**

***Index Terms* - Hopping robot; Motion planning; Under-actuation; Optimization**

I. INTRODUCTION

The legged hopping or running robot was studied extensively in the past two decades. Raibert and his co-workers have significant contributions on showing the dynamic balance and motion control principle exampled by their 2D[1] and 3D[2] one-legged hopping robot, two legs [3] and four legs [4] running robot. The regulable step length and intermittent supported manner tend the dynamic legged robot to fit natural terrain better than wheeled or tracked vehicles. In flight phase, there is no external force except gravity applied to the hopping/running robots, the system bears "constraints" expressed by angular momentum conservation that is nonholonomic [5,6]. The hopping/running robot is also a high-speed dynamic mechanical system where real-time controller and great energy efficiency is necessary [7,8]. Encouraged by these features of the hopping/running robot in biomechanics, constraint dynamics, and control technique for nonholonomic systems, the one-legged hopping robot, can be seen a fundamental prototype for dynamic walking robot [9] or legged running robot [4], is the research object in this paper.

There are many hopping robots have been presented so far [10-14]. The one-legged robot is the primary research prototype for hopping robot as mentioned above, and the model of the prototypes described principally by Spring Loaded Inverted Pendulum [2-8,13-15]. The SLIP model based hopping robots permit to analyze and control the system without considering the dynamic coupling of the mechanical systems. Though the control problem is simplified, even a linear time-invariant feedback based controller can stabilize the robots to their periodic gaits [1-4], and the nonlinear dynamic behaviors of the periodic motion can be revealed more thoroughly [15] for the simplest mechanical system. Nevertheless, from the point of view of biomechanics, the nonlinear dynamic coupling of the multi degree of freedoms mechanical system is useful in some cases. For instance, athlete swing arm can help balance and speed in walking or running, the strong tail of some animals such as leopards, lions, and kangaroos plays an important role for running or changing the run direction. In this paper, a new one-legged hopping robot with non-SLIP model is investigated for understanding the dynamic coupling of the system. Since the robot has a passive spring leg, it is true an underactuated mechanical system that can but be controlled by the internal dynamic coupling.

II. STANCE BALANCE MANIFOLD

Fig. 1 shows the planar robot prototype (a) and its mechanism model (b) considered in this paper. The robot consists of two actuated arms and one passive telescopic spring leg. The leg is composed of two segments. One segment of the leg is nonzero mass and another is massless. The length of the segment with nonzero mass is l_1, the mass of it is m_1, and the COM lies in the middle of the length. The massless segment has length, l_2, is connected to the former by linear spring serially with same axis line. The stiffness of the linear spring is k. The length and the mass of the two arms are r and m_2 respectively. Given the COM of the arm lies at its end for simplifying the formulations. The two arms are hinged at the top of the nonzero mass segment of leg. Defining the general coordinates of the model are $(x_0, z_0, l_2, \varphi, \theta_1, \theta_2)$, of which (x_0, z_0) is the position of the foot toe in the vertical plane, l_2 is the length of the massless leg ($l_2 = l_0$ when the spring is free, $l_2 = l_{20}$ when the leg is stance vertically with static balance.), φ is the angle between leg's axis line and horizontal plane, θ_1, θ_2 are angles of the two arms with respect to the leg respectively. Positive direction of all angles

* This work is partially supported by NSFC with No.50475177, Beijing NSF with No.3062009 and CPSF with No. 20070410001 to G-P. He.

is defined as anticlockwise. Based on these definitions, the kinematics of the COM of the system can be expressed as

$$\boldsymbol{X}_C = \boldsymbol{f}(x_0, z_0, l_2, \varphi, \theta_1, \theta_2) \tag{1}$$

where $\boldsymbol{X}_C = [x_C \quad z_C]^{\mathrm{T}}$ is the position of COM in vertical plane.

The steady motion of a one-legged robot includes two motion phases, stance phase and flight phase. In stance phase, since x_0 and z_0 become to constants, the kinematics of the COM (1) can be rewritten as

$$\boldsymbol{X}_C = \boldsymbol{f}_1(\boldsymbol{q}_1) \tag{2}$$

where $\boldsymbol{q}_1 = [l_2 \quad \varphi \quad \theta_1 \quad \theta_2]^{\mathrm{T}}$, the generalized coordinates of the robot in stance phase. Specifically, the equation (2) is of the form

$$x_C = \frac{1}{m_1 + 2m_2}\Big[m_1(\frac{1}{2}l_1 + l_2)\cos\varphi + 2m_2(l_1 + l_2)\cos\varphi + m_2 r\cos(\varphi + \theta_1) + m_2 r\cos(\varphi + \theta_2)\Big] \tag{3}$$

$$z_C = \frac{1}{m_1 + 2m_2}\Big[m_1(\frac{1}{2}l_1 + l_2)\sin\varphi + 2m_2(l_1 + l_2)\sin\varphi + m_2 r\sin(\varphi + \theta_1) + m_2 r\sin(\varphi + \theta_2)\Big] \tag{4}$$

(a)

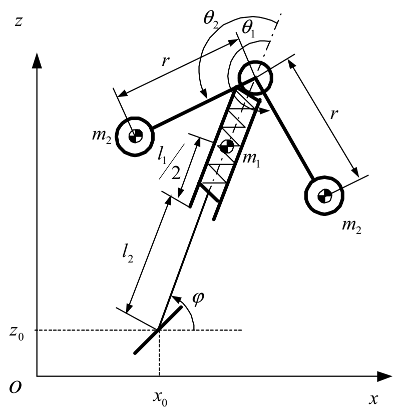

(b)

Fig. 1. The robot prototype (a) and mechanism model (b).

Let $x_C = 0$, equation (3) describes the balance manifold of the robot. Given different angles φ, the corresponding balance manifolds can be drawn in Fig. 2. Where Fig. 2 (b) corresponding to $\varphi = \pi/2$ shows a connected manifold that is perfect for stance balance. When $\varphi \neq \pi/2$, the balance manifolds depicted by Fig. 2 (a) and (c) show discrete feature, and the region of the manifold shrinks along with the angle φ deviating from vertical position. As to a SLIP model based hopping robot, the stance balance manifold can appear at $\varphi = \pi/2$, but absence at all points with $\varphi \neq \pi/2$. A larger balance region in stance phase for a non-SLIP hopping robot tends the system to be stabilized easily [12]. And more important, holding a balance manifold means many configurations can balance the system. Thus, one can select an optimal configuration in some sense such as the lowest configuration for traveling where obstacles are closely spaced, or a configuration where the joint limits can be avoided. The later case is considered in section 4 of the present paper.

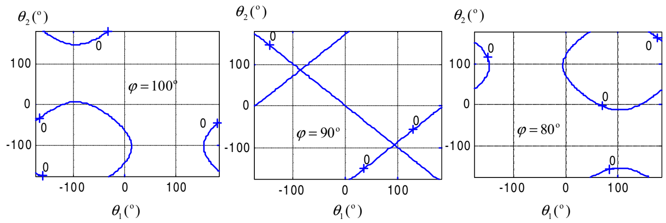

(a) (b) (c)

Fig. 2. The balance manifolds in stance phase

III. Features of The Dynamic Coupling

The features of the dynamic coupling of an underactuated robot system are important for motion controlling. For insight into this, we need the dynamics of the system. In stance phase, the dynamics can be written as

$$\boldsymbol{M}_1\ddot{\boldsymbol{q}}_1 + \boldsymbol{C}_1 = \boldsymbol{Q}_1 \tag{5}$$

where $\boldsymbol{q}_1 = [l_2 \quad \varphi \quad \theta_1 \quad \theta_2]^{\mathrm{T}}$, $\boldsymbol{M}_1$ is the inertia matrix, $\boldsymbol{C}_1$ includes centrifugal and Coriolis torques, gravity, friction, and spring force. $\boldsymbol{Q}_1 = [0 \quad 0 \quad \tau_1 \quad \tau_2]^{\mathrm{T}}$ is the generalized driver force vector in which the former two zero elements means the leg is unactuated and there is no external torque applied to the foot. τ_1 and τ_2 are drivers torque of the two arms respectively. In flight phase, the dynamics of the system can be given by

$$\boldsymbol{M}_2\ddot{\boldsymbol{q}}_2 + \boldsymbol{C}_2 = \boldsymbol{Q}_2 \tag{6}$$

where $\boldsymbol{q}_2 = [x_0 \quad z_0 \quad \varphi \quad \theta_1 \quad \theta_2]^{\mathrm{T}}$, $\boldsymbol{M}_2$ also a inertia matrix, $\boldsymbol{C}_2$ is similar to $\boldsymbol{C}_1$ of equation (5) but friction and spring forces of the leg are absent. $\boldsymbol{Q}_2 = [0 \quad 0 \quad 0 \quad \tau_1 \quad \tau_2]^{\mathrm{T}}$ is the generalized non-conservation driver forcer, of which the former three zero elements mean no non-conservation forces corresponding to the generalized coordinates x_0, z_0 and φ. One can refer to [16] for the detailed forms of equations (5) and (6), which can be rewritten to a uniform expression

$$\begin{aligned} \boldsymbol{m}_{pp}\ddot{\boldsymbol{q}}_p + \boldsymbol{m}_{pa}\ddot{\boldsymbol{q}}_a + \boldsymbol{c}_p = \boldsymbol{0} \\ \boldsymbol{m}_{ap}\ddot{\boldsymbol{q}}_p + \boldsymbol{m}_{aa}\ddot{\boldsymbol{q}}_a + \boldsymbol{c}_a = \boldsymbol{\tau} \end{aligned} \tag{7}$$

where $\boldsymbol{M} = \begin{bmatrix} \boldsymbol{m}_{pp} & \boldsymbol{m}_{pa} \\ \boldsymbol{m}_{ap} & \boldsymbol{m}_{aa} \end{bmatrix}$ is the inertial matrix. In stance phase, $\boldsymbol{M} = \boldsymbol{M}_1$, $\boldsymbol{q}_p = [l_2 \quad \varphi]^{\mathrm{T}}$, $\boldsymbol{q}_a = [\theta_1 \quad \theta_2]^{\mathrm{T}}$, $\boldsymbol{C}_1 = [c_{\mathrm{p}}^{\mathrm{T}} \quad c_{\mathrm{a}}^{\mathrm{T}}]^{\mathrm{T}}$, $\boldsymbol{\tau} = [\tau_1 \quad \tau_2]^{\mathrm{T}}$. In flight phase, $\boldsymbol{M} = \boldsymbol{M}_2$, $\boldsymbol{q}_p = [x_0 \quad z_0 \quad \varphi]^{\mathrm{T}}$, $\boldsymbol{q}_a = [\theta_1 \quad \theta_2]^{\mathrm{T}}$, $\boldsymbol{C}_2 = [c_{\mathrm{p}}^{\mathrm{T}} \quad c_{\mathrm{a}}^{\mathrm{T}}]^{\mathrm{T}}$, $\boldsymbol{\tau} = [\tau_1 \quad \tau_2]^{\mathrm{T}}$. The first equation of (7) corresponds to the coupling dynamics of the underactuated hopping robot showing to be the nonholonomic constraints of the system [5,6,16]. We focus on the acceleration relationship between the active and the passive generalized coordinates, rewriting the first line of equation (7) as

$$\ddot{\boldsymbol{q}}_p = \boldsymbol{m}_E\ddot{\boldsymbol{q}}_a \tag{8}$$

where $\boldsymbol{m}_E = -\boldsymbol{m}_{pp}^{-1}\boldsymbol{m}_{pa}$ and $\ddot{\bar{\boldsymbol{q}}}_p = \ddot{\boldsymbol{q}}_p + \boldsymbol{m}_{pp}^{-1}\boldsymbol{c}_p$ are substituted with considering $\boldsymbol{m}_{pp}$ being a symmetric positive-definite matrix. The acceleration $\ddot{\bar{\boldsymbol{q}}}_p$ can be viewed as a virtual acceleration of the passive generalized coordinates, generated by the accelerations of the active ones, and by the nonlinear torques due to velocity effects. The matrix $\boldsymbol{m}_E$, indicates the coupling of the active and the passive accelerations, is important in understanding of how an underactuated system works. We employee the definition of dynamic coupling index (DCI) for underactuated manipulators proposed by Bergermann et al. [17], the DCI for the underactuated hopping robot can be defined as

$$\rho = \prod_{i=1}^{s} \sigma_i \tag{9}$$

where $\sigma_1 \geq \sigma_2 \geq \cdots \geq \sigma_s$, and σ_i denotes the singular values of matrix $\boldsymbol{m}_E$. The DCI described by equation (9) can be utilized to measure the controllability of the system in specific configuration since singular values of matrix $\boldsymbol{m}_E$ quantify the capacity to "transmit" the acceleration from active to passive coordinate. The feature of the dynamic coupling of the robot prototype shown in Fig. 1 is plotted in Fig. 3, where the model parameters of the robot prototype are listed in the Appendix of [16]. Since the matrix $\boldsymbol{m}_E$ is independent of the leg angle φ [16], and the length of the massless leg is approximated to l_{20}, the DCI depends only on the configuration of the two arms. Refer to Fig. 3, the maximal dynamic coupling configurations $[\theta_1 \quad \theta_2]^{\text{opt}} \approx [97^{\text{o}} \quad -97^{\text{o}}]$ and $[\theta_1 \quad \theta_2]^{\text{opt}} \approx [-97^{\text{o}} \quad 97^{\text{o}}]$ are easy to be found out.

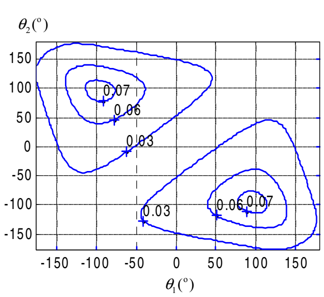

Fig. 3. The dynamic coupling measure in stance phase

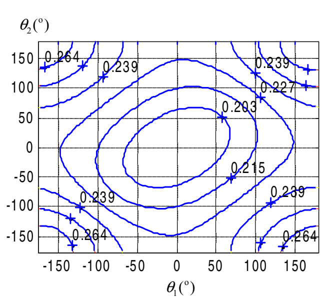

Fig. 4. The dynamic coupling measure of flight phase

In the flight phase, the angle of the leg should be controlled to its expected position for preparing the next stance phase. It is well known that the motion of COM of the hopping robot cannot be controlled during flight phase because of the linear momentum conservations and shows a parabolic trajectory. The dynamic coupling equation of (7) in flight phase can be rewritten as

$$m_{H1}\ddot{\varphi} + m_{H2}\ddot{\theta}_1 + m_{H3}\ddot{\theta}_2 + c_H = 0 \tag{10}$$

where m_{H1}, m_{H2}, m_{H3} and c_H are the equivalent quantities of the corresponding elements of the first line of equation (7). Similar to (8), equation (10) can be rewritten as

$$\ddot{\bar{\varphi}} = \ddot{\varphi} + \frac{c_H}{m_{H1}} = -\frac{m_{H2}}{m_{H1}}\ddot{\theta}_1 - \frac{m_{H3}}{m_{H1}}\ddot{\theta}_2 \tag{11}$$

where $m_{H1} \neq 0$ is the inertial parameter of the leg. Since the dynamic coupling matrix $\boldsymbol{m}_E = \begin{bmatrix} \frac{m_{H2}}{m_{H1}} & \frac{m_{H3}}{m_{H1}} \end{bmatrix}$ is always full rank, $\text{rank}(\boldsymbol{m}_E) \equiv 1$, the unique singular value σ of the matrix $\boldsymbol{m}_E$ satisfies $\sigma \equiv 1$, the DCI (9) cannot show the detailed feature of dynamic coupling of flight phase. Differing from the definition (9), the DCI in flight phase is defined as

$$\rho = |m_{H2}m_{H3}| / (m_{H1})^2 \tag{11}$$

The distribution of dynamic coupling measured by equation (11) for the robot prototype is depicted in the Fig. 4. One can find the measure ρ always satisfying $\rho > 0$ with showing slightly changes in different configurations of the robot arms.

IV. Optimal Motion Planning And Control

A. Motion planning and control for vertical hopping

Taking into account the results given by section 1 and 2, one can drive the motion of the arms near to its maximum dynamic coupling configuration, and simultaneously, on its balance manifold. Apparently these will result in the least energy expenditure and more robust balance capability. Considering vertical hopping control problem, the optimal motion planning can be described as: (1) Control the orientation of leg to vertical position, $\varphi^{\text{d}} = 90^{\text{o}}$, where the robot has a balance manifold with wider range in stance phase; (2) Control the two arms to their maximal dynamic coupling configuration $[\theta_1 \quad \theta_2]^{\text{d}} \approx [\theta_1 \quad \theta_2]^{\text{opt}}$, where the best controllability of the system is achieved. (3) Control the vibration of the leg to resonance, which is described by

$$l_2^{\text{d}} = l_{20} + A(t)\sin(\omega_n(t - T_k) + \beta) \tag{12}$$

where $A(t)$ is the vibration amplitude. For the prototype shown in Fig. 1, the maximal amplitude is $A_{\max} \approx 3.5(l_0 - l_{20})$. T_k is the touchdown time of the k-th times jump. ω_n is the nature angular frequency of the system. β is the phase angle. The phase angle β is defined by the initial position of the spring in leg. Given the initial displacement of spring is Δl and current vibration amplitude of spring is $A(t)$, the phase angle can be calculated by

$$\beta = -\arcsin(\Delta l / A(t)), \quad \Delta l = (l_0 - l_{20}) > 0 \tag{13}$$

The adopted control law is an improved version of it in [16], in which the control law is designed by position feedback of the COM. Since the inverse solutions of equation (3) are multiple, the configuration of the two arms is not definite. This drawback is overcome by the optimal motion plan presented above. Considering the first equation of (7), the new control law during stance phase has a form

$$\boldsymbol{u} = \boldsymbol{H}_2\boldsymbol{H}^+ \begin{bmatrix} \dot{\boldsymbol{q}}_{\text{a}}^{\text{d}} + k_1\boldsymbol{e}_{\text{a}} + k_2\int \boldsymbol{e}_{\text{a}}\,\text{d}t \\ -(\boldsymbol{m}_{\text{pa}})^+ \left[\boldsymbol{m}_{\text{pp}}\left(\ddot{\boldsymbol{q}}_{\text{p}}^{\text{d}} + k_3\dot{\boldsymbol{e}}_{\text{p}} + k_4\boldsymbol{e}_{\text{p}}\right) - \boldsymbol{c}_{\text{p}}\right] \end{bmatrix} \tag{14}$$

where $(\cdot)^{+}$ denotes the Moore-Penrose generalized inverse of the matrix. Input $\boldsymbol{u}=\ddot{\boldsymbol{q}}_{\mathrm{a}}$, $k_i>0, i=1,2,3,4$. $\boldsymbol{q}_{\mathrm{a}}^{\mathrm{d}}=\begin{bmatrix}\theta_1^{\mathrm{d}} & \theta_2^{\mathrm{d}}\end{bmatrix}^{\mathrm{T}}$ is the desired position of arms, $\boldsymbol{q}_{\mathrm{p}}^{\mathrm{d}}=\begin{bmatrix}l_2^{\mathrm{d}} & \varphi^{\mathrm{d}}\end{bmatrix}^{\mathrm{T}}$ is the planed passive coordinates. $\boldsymbol{H}_1 \in \mathrm{R}^{\mathrm{n_a}\times \mathrm{r}}$, $r \geq 2n_a$ is a constructed smooth time-varying matrix that can be differentiated respect to time with showing $\boldsymbol{H}_2=\mathrm{d}\boldsymbol{H}_1/\mathrm{d}t$. The combined matrix $\boldsymbol{H}=\begin{bmatrix}\boldsymbol{H}_1\\ \boldsymbol{H}_2\end{bmatrix}\in \mathrm{R}^{2\mathrm{n_a}\times \mathrm{r}}$ must be full rank, viz. $\operatorname{rank}(\boldsymbol{H})=2n_a$.

Considering the equation (10), the new control law during flight phase has a form

$$\boldsymbol{u}=\boldsymbol{H}_2\boldsymbol{H}^{+}\begin{bmatrix}\dot{\boldsymbol{q}}_{\mathrm{a}}^{\mathrm{d}}+k_5\boldsymbol{e}_a+k_6\int \boldsymbol{e}_a\mathrm{d}t\\ -\begin{bmatrix}m_{H2} & m_{H3}\end{bmatrix}^{+}\left[m_{H1}\left(\ddot{\varphi}^{d}+k_7\dot{e}_{\varphi}+k_8e_{\varphi}\right)-c_H\right]\end{bmatrix} \tag{15}$$

where $\boldsymbol{e}_a=\begin{bmatrix}\dot{\theta}_1^{\mathrm{d}} & \dot{\theta}_2^{\mathrm{d}}\end{bmatrix}^{\mathrm{T}}-\begin{bmatrix}\dot{\theta}_1 & \dot{\theta}_2\end{bmatrix}^{\mathrm{T}}$, $e_{\varphi}=\varphi^{\mathrm{d}}-\varphi$, $k_i>0, i=5,6,7,8$. With the model parameters listed in Appendix of [16], the numerical simulation of vertical hoping with varying height is shown in Fig. 5. The Fig. 5(a) and Fig. 5 (b) show the orientation of the robot is stabilized to $\begin{bmatrix}\varphi & \theta_1 & \theta_2\end{bmatrix}=\begin{bmatrix}90^{\circ} & 97^{\circ} & -97^{\circ}\end{bmatrix}$. Fig. 5 (c) shows the vibration of the spring leg and the hopping height of the foot tip. Fig. 5 (d) depicts the drivers' torque of the arms.

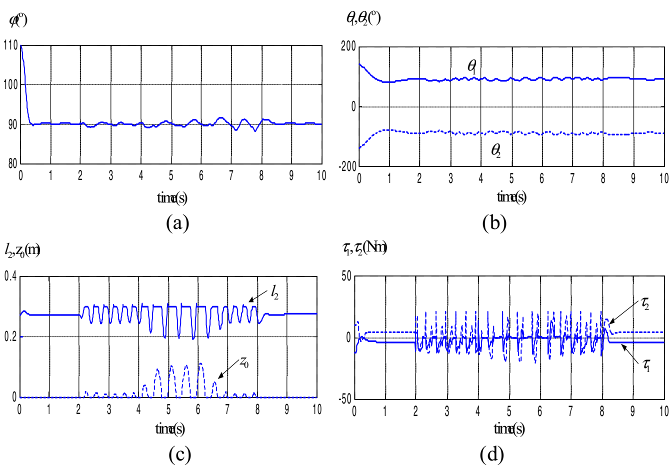

Fig. 5. Vertical hopping control

B. Motion planning and control for planar hopping

Provided that swing angle of the leg is not large in running [8], the duration of stance phase can be calculated with referring to Fig. 6, in which the abscissa is time and the ordinate denotes the length of the telescopic leg l_2 . In the Figure, l_0 and l_{20} are the length of l_2 with spring free and gravity balance respectively. $l_2^{\min}$ denotes the minimal length of l_2 , thus $\Delta l_2^{\max}=l_0-l_2^{\min}$ is the maximal deformation of the linear spring. A denotes the vibration amplitude of the spring leg with range $A\in\left(l_0-l_2^{\min} \quad l_{20}-l_2^{\min}\right)$ for our robot.

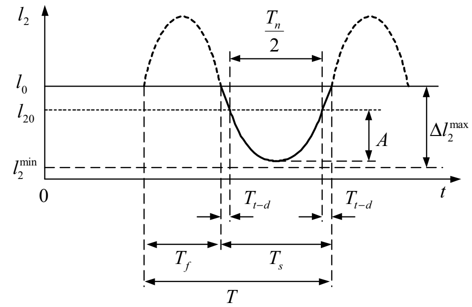

Fig. 6. The time analysis of stance phase

The duration of stance phase is

$$T_s=\frac{T_n}{2}+2T_{t-d}=\frac{T_n}{2}\left(1+\frac{l_0-l_{20}}{A}\right),\ A>l_0-l_{20} \tag{16}$$

where $T_n=2\pi/\omega_n$ is the natural vibration period of the spring leg, while $\omega_n=\sqrt{k/m}$ is the natural angular frequency. k,m express the stiffness and the total mass of the system respectively. If let x_s and x_f express the moving distance of COM during stance phase and flight phase respectively, and h_0 and h express the lift-off height and maximum height of the COM during a hopping period respectively. The duration of flight phase can be written as

$$T_f=2\sqrt{\frac{2(h-h_0)}{g}}=\frac{2\dot{z}_{C0}}{g} \tag{17}$$

where $\dot{z}_{C0}$ denotes the lift-off speed in vertical direction, g is the gravitational acceleration. Taking into account the equations (16) and (17), and supposing the average moving speed in horizontal direction is $\dot{x}_{C0}$, the displacement during a hopping period is expressed by

$$\Delta x=x_s+x_f=\dot{x}_{C0}\left(T_s+T_f\right) \tag{18}$$

It is presumed that the energy loss can be fully compensated during the stance, the angular momentum at lift-off is negligible, and then the relationship between the kinetic energy at lift-off and the maximal potential energy of spring is

$$E_{\text{spring}}=\frac{1}{2}kA^2=\frac{1}{2}m\left[\left(\dot{x}_{C0}\right)^2+\left(\dot{z}_{C0}\right)^2\right] \tag{19}$$

By equation (19), the vertical lift-off speed $\dot{z}_{C0}$ can be resolved to

$$\dot{z}_{C0}=\sqrt{\frac{k}{m}A^2-\dot{x}_{C0}} \tag{20}$$

where $\dot{z}_{C0}\geq 0$ is considered. Using the equations (16), (17) and (19), equation (18) can be rewritten as

$$\Delta x=\dot{x}_{C0}\left(T_s+\frac{2}{g}\sqrt{\frac{k}{m}A^2-\dot{x}_{C0}}\right) \tag{21}$$

Referring to equation (16), where T_s is a constant when the vibration amplitude A is fixed at steady motion, thus the displacement Δx is a function about the average speed $\dot{x}_{C0}$ only. For a given A , the maximal average moving speed $\dot{x}_{C0}$

can be given by $\mathrm{d}\Delta x/\mathrm{d}\dot{x}_{C0} = 0$, and the maximum is expressed by

$$\left|\dot{x}_{C0}\right|^{\mathrm{opt}} = T_s g A \sqrt{\frac{k}{m(4+T_s^{\,2}g^2)}} \tag{22}$$

For our robot prototype, the relationship between the maximal average moving speed and the vibration amplitude of the leg spring is drawn in Fig. 7, where the abscissa is a coefficient given by, the ordinate shows the lift-off speeds $\left|\dot{x}_{C0}\right|^{\mathrm{opt}}, \dot{z}_{C0}\,(\mathrm{m/s})$ and hopping height $\Delta h = h - h_0$ simultaneously. According to the numerical results, the maximal average speed $\left|\dot{x}_{C0}\right|^{\mathrm{opt}}$ gets to 1.3(m/s) when $\lambda = 3.5$ (viz. $A = 3.5(l_0 - l_{20}) \approx 0.096\mathrm{m}$) is achieved. The Fig. 8 shows the relationship between the hopping period $T = T_a + T_f$ and the vibration amplitude A, where the maximal average moving speed is also considered. One can find that the hopping period T increases along with the augmentation of vibration amplitude.

For a given value A, since the maximal average moving speed $\left|\dot{x}_{C0}\right|^{\mathrm{opt}}$ is defined by the equation (22), and the duration T_s is defined by equation (16), referring to the Fig. 9, the swing angle of the leg can be calculated by

$$\Delta\varphi^{\mathrm{opt}} = \arcsin\left(\frac{\left|\dot{x}_{C0}\right|^{\mathrm{opt}} T_s}{2 l_C}\right) \tag{23}$$

where

$$l_C = \sqrt{x_C^{\,2} + z_C^{\,2}}\,\Big|_{(\theta_1,\theta_2)=(97^\circ,-97^\circ)} \approx 0.8095(l_1 + l_2) \tag{24}$$

In equation (24), l_C is defined to the equivalent length of leg, which is the distance between the COM of the system and the foot tip. Generally, the position of COM varies, thus the equivalent length l_C is a variable. Nevertheless, when the two arms are controlled to their maximum dynamic coupling configurations $[\theta_1 \quad \theta_2]^{\mathrm{opt}}$, l_C can be calculated by equation (24). In fact, the swing angle of the leg expressed by (23) is the optimal lift-off and touchdown angle of the leg because that the greatest dynamic coupling configuration $[\theta_1 \quad \theta_2]^{\mathrm{opt}}$ is selected to achieve the maximal average moving speed $\left|\dot{x}_{C0}\right|^{\mathrm{opt}}$. In this case, the planned motion has the greatest energy efficiency [8]. For the prototype shown in Fig. 1, the relationship between the optimal swing angle $\Delta\varphi^{\mathrm{opt}}$ and the vibration amplitude A is shown in Fig. 10 numerically.

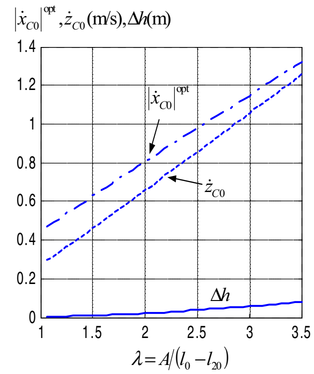

Fig.7. The relationship between the maximal hopping speed and the vibration amplitude of the spring leg.

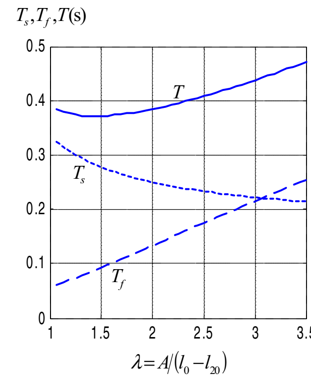

Fig. 8. The relationship between the hopping period and the vibration amplitude of the spring leg

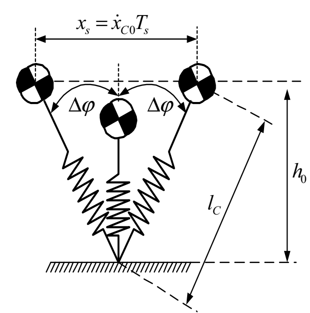

Fig. 9. A sketch for calculating the swing angle of leg

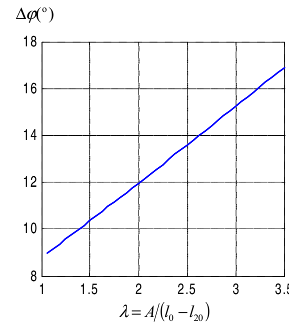

Fig. 10. The relationship between the optimal swing angle of leg and the vibration amplitude

The control laws given by equations (14) and (15) are still adopted for planar hopping, but the commanded angular position of the leg is changed to $\varphi^{\mathrm{d}} = 90^\circ + \Delta\varphi^{\mathrm{opt}}$ for stance phase, $\varphi^{\mathrm{d}} = 90^\circ - \Delta\varphi^{\mathrm{opt}}$ for flight phase, or interchange the commanded angular position for hopping with reverse direction. Fig. 11 shows a 30s simulation sequence of planar hopping in which the desired moving speed is adjusted a number of times (Refer to Fig. 11 (a)). Since configuration space feedback is used in the control laws (14) and (15), the hopping speed and displacement are approximate (Fig. 11 (b)). Nevertheless, referring to Fig. 11 (c), it is important that the robot can be stabilized to their desired configuration. In order to show the steady hopping clear, Fig. 12 depicts two periods of hopping procedure during 20s-21s with data from Fig. 11. Fig. 12 (c) shows the changes of the orientation of the robot relative to the reference point $[\varphi, \theta_1, \theta_2] = [90^\circ, 97^\circ, -97^\circ]$. A careful observation of this figure shows that the movement of the two arms has reversed angle phase, and the rhythmic activation of the two arms excite resonant oscillations in the spring-mass system formed by the two arms and leg, showing a reasonable motion style on intuition.

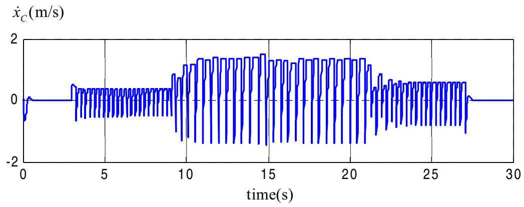

(a) The moving speed in horizontal direction

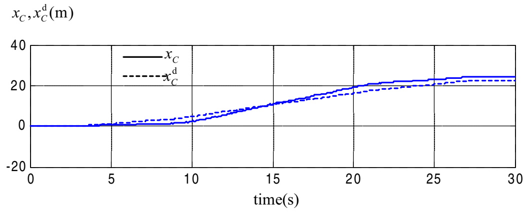

(b) The moving distance of the COM of the robot in planar hopping control

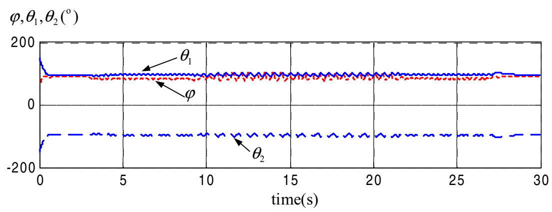

(c) The posture of the robot in planar hopping control

Fig. 11. The simulation results of planar hopping with changing the moving speed several times.

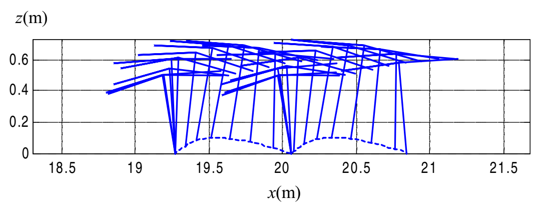

(a)

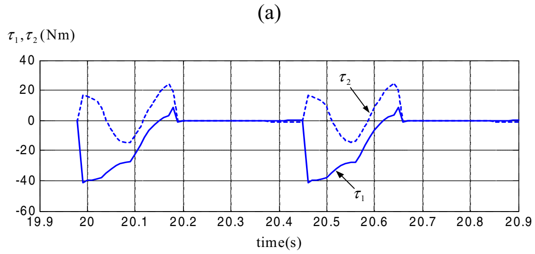

(b)

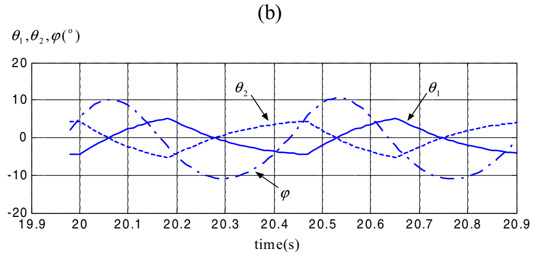

(c)

Fig. 12. Two hopping periods motion with data from Fig. 16 during the motion at the great moving speed ($\dot{x}_C \approx 1.2\text{m/s}$).

V. Conclusions

It is revealed that the non-SLIP model based one-legged hopping robot holds stance balance manifold that can provide better balance capability. Based on the dynamic coupling analysis, an optimal motion-planning algorithm is presented for energy efficiency control of the underactuated system with considering the nonholonomic constraints. The dexterous mobility of the robot has been shown by some detailed numerical simulation results. These results also show the important role of dynamic coupling for the underactuated, failed actuators contained, or weight restricted mechanical system.

References

[1]. M. H. Raibert, Hopping in Legged Systems-Modeling and Simulation for the Two-Dimensional One-Legged Case, IEEE Transaction on Systems, Man, and Cybernetics, 1984, SMC-14 (3): 451-463.

[2]. M. H. Raibert, H. Benjamin Brown, Jr. and M. Chepponis, Experiments in Balance with a 3D One-Legged Hopping Machine, The International Journal of Robotics Research, 1984, 3(2): 75-92.

[3]. J. K. Hodgins and M. H. Raibert. Adjusting Step Length for Rough Terrain Locomotion, IEEE Transactions on Robotics and Automation, 1991, 7(3): 289-298.

[4]. M.H. Raibert, M. Chepponis, and H. B. Brown, JR. Running on Four Legs As Though They Were One, IEEE Journal of Robotics and Automation, 1986, RA-2 (2): 70-82.

[5]. F. ur-Rehman. Steering Control of A Hopping Robot Model During The Flight Phase, IEE Proc.-Control Theory Appl. 2005, 152(6): 645-653.

[6]. Y.P. Tian and S.H. Li. Exponential Stabilization of Nonholonomic Dynamic Systems by Smooth Time-Varying Control, Automatica, 2002, 38:1139-1146.

[7]. M. Ahmadi and M. Buehler, The ARL Monopod II Running Robot: Control and Energetics, IEEE International Conference on Robotics and Automation, Michigan, May, 1999,1689-1694.

[8]. E. Papadopoulos and N. Cherouvim. On Increasing Energy Autonomy for a One-Legged Hopping Robot, IEEE International Conference on Robotics and Automation, New Orleans, LA, April 2004, 4645-4650.

[9]. S. Collins, A. Ruina, R. Tedrake and M Wisse, Efficient Bipedal Robots Based on Passive-Dynamic Walkers, Science, 2005,307:1082-1085.

[10]. F. Iida, R. Dravid and C. Paul. Design and Control of a Pendulum Driven Hopping Robot, IEEE/RSJ International Conference on Intelligent Robots and Systems, Lausanne, Switzerland, October 2002, 2141-2146.

[11]. S. H. Hyon and T. Mita, Development of a Biologically Inspired Hopping Robot-"Kenken", IEEE International Conference on Robotics and Automation, Washington, DC, May 2002, 3984-3991.

[12]. J. Leavitt, J. E. Bobrow and A. Sideris. Robust Balance Control of a One-Legged, Pneumatically-actuated, Acrobot-like Hopping Robot, IEEE International Conference on Robotics and Automation, New Orleans, April, 2004, 4240-4245.

[13]. G. Zeglin, The Bow Leg Hopping Robot, Doctor Dissertation, Carnegie Mellon University, 1999.

[14]. M, Ahmadi and M. Buehler. Controlled Passive Dynamic Running Experiments With The ARL- Monopod II, IEEE Transactions on Robotics and Automation, 2006, 22(5): 974-986.

[15]. R.T. M'Closkey and J.W. Burdick. Periodic Motions of a Hopping Robot With Vertical and Forward Motion, The International Journal of Robotics Research, 1993, 12(3): 197-218.

[16]. G.P. He, X.L. Tan, X.H. Zhang and Z. Lu. Modeling, Motion Planning, and Control of One-Legged Hopping Robot Actuated by Two Arms, to appear in Mechanism and Machine Theory.

[17]. M. Bergerman, C. Lee and Y. Xu. Dynamic Coupling of Underactuated Manipulators, IEEE Conference on Robotics and Automation, 1995, 500-505.